

# Space-VLBI observations of OH maser OH34.26+0.15: low interstellar scattering

V.I. Slysh,<sup>1</sup> M.A. Voronkov,<sup>1</sup> V. Migenes,<sup>2</sup> K.M. Shibata,<sup>3</sup> T. Umemoto,<sup>3</sup> V.I. Altunin,<sup>4</sup> I.E. Val'tts,<sup>1</sup> B.Z. Kanevsky,<sup>1</sup> M.V. Popov,<sup>1</sup> A.V. Kovalenko,<sup>1</sup> E.B. Fomalont,<sup>5</sup> B.A. Poperechenko,<sup>6</sup> Yu.N. Gorshenkov,<sup>6</sup> B.R. Carlson,<sup>7</sup> S.M. Dougherty,<sup>7</sup> J.E. Reynolds,<sup>8</sup> D.R. Jiang,<sup>9</sup> A.I. Smirnov<sup>1</sup> and V.G. Grachev<sup>10</sup>

<sup>1</sup>*Astro Space Centre of Lebedev Physical Institute, Profsoyuznaya 84/32, 117810 Moscow, Russia*

<sup>2</sup>*University of Guanajuato, Department of Astronomy, Apdo Postal 144, Guanajuato, CP36000, GTO, Mexico*

<sup>3</sup>*National Astronomical Observatory, 2-21-1 Osawa, Mitaka, Tokyo 181, Japan*

<sup>4</sup>*Jet Propulsion Laboratory, 4800 Oak Grove Dr., Pasadena, CA 91109, USA*

<sup>5</sup>*National Radio Astronomy Observatory, 520 Edgemont Rd., Charlottesville, VA 22903, USA*

<sup>6</sup>*Special Research Bureau, Moscow Power Engineering Institute, Krasnokazarmennaya st. 14, 111250 Moscow, Russia*

<sup>7</sup>*Dominion Radio Astrophysical Observatory, Herzberg Institute of Astrophysics, National Research Council, PO Box 248, Penticton, BC, Canada V2A 6K3*

<sup>8</sup>*Australia Telescope National Facility, PO Box 76, Epping, NSW 2121, Australia*

<sup>9</sup>*Shanghai Astronomical Observatory, 80 Nandan Rd, Shanghai 200080, China*

<sup>10</sup>*Institute of Applied Astronomy, Zhdanovskaya str. 8, 197042 St.Petersburg, Russia*

Received date; accepted date

## ABSTRACT

We report on the first space-VLBI observations of the OH34.26+0.15 maser in two main line OH transitions at 1665 and 1667 MHz. The observations involved the space radiotelescope on board the Japanese satellite *HALCA* and an array of ground radio telescopes. The map of the maser region and images of individual maser spots were produced with an angular resolution of 1 milliarcsec which is several times higher than the angular resolution available on the ground. The maser spots were only partly resolved and a lower limit to the brightness temperature  $6 \times 10^{12}$  K was obtained. The maser seems to be located in the direction of low interstellar scattering, an order of magnitude lower than the scattering of a nearby extragalactic source and pulsar.

**Key words:** ISM: molecules – stars: formation – H II regions – masers – scattering

## 1 INTRODUCTION

OH masers were the first to be discovered as a new class of astronomical phenomena exhibiting intense, narrow band, polarized, variable emission in interstellar molecular transitions (Weaver et al. 1965). The source of this emission was shown to be small, compact clumps of neutral gas, at the periphery of compact H II regions created by newly born massive O-stars. Another class of OH masers is related to evolved low- and medium-mass stars, and is not considered here. High angular resolution study of OH masers showed that they consist of a number of bright compact maser spots separated by several arcseconds. The spots themselves are from 2 to 70 milliarcseconds in extent, and in some masers are barely resolved, even with the highest angular resolution available from ground based VLBI arrays (Moran et al. 1968).

The goal of the high angular resolution study of OH masers is to determine relative position of the spots, to measure the intensity, and to map the spots. Determination of the size and the shape of the maser spots would be very helpful for understanding the maser emission mechanism and its limiting brightness temperature. The shape of the maser spots may be indicative of the type of physical phenomena responsible for the origin of the maser emission.

Several possible sites for the origin of maser emission; such as the shocks at the border of H II regions, or the interaction region between a molecular outflow and ambient molecular clouds, as well as protoplanetary accretion disks around young star, have been suggested. The maser spot shape and size are important properties of the maser emission, provided they are intrinsic to the source, and not caused by a propagation effect such as interstellar scattering.

There is a widespread opinion that OH masers are heavily scattered by interstellar turbulence, and that observed images of maser spots are scattering broadened images of essentially point-like sources. This view is based on data obtained from the study of scattering of pulsars and continuum sources. The importance of scattering for OH masers is due to their location within the thin galactic disk where the scattering is most severe. The first observational evidence for the scattering of OH masers obtained by direct VLBI measurements came from Kembell, Diamond and Mantovani (1988). They measured the size of the strongest spectral features in 16 galactic masers using a single-baseline interferometer with a fringe spacing of 5 milliarcsec. Only three masers out of 16 observed have shown compact details, less than 2.5 milliarcsec in size. The rest of the masers were completely resolved implying angular size larger than 5 milliarcsec. Kembell et al. (1988) concluded that their results were consistent with the interstellar scattering angle of about 20 milliarcsec derived from pulsar scattering data, and with the clumpy distribution of electron density fluctuations which are responsible for the large spread of measured angular sizes. Hansen et al. (1992) made a VLBI survey of interstellar broadening of 20 galactic OH masers, using a 7-station VLBI array. They found a large range of angular sizes from  $0.8 \pm 0.5$  milliarcsec to  $74 \pm 7$  milliarcsec in their sample of OH masers. They fitted the angular size  $\theta$  versus distance  $D$  dependence by a relation  $\theta \sim D^{0.65}$  which is close to the expected scaling with distance for homogeneous turbulence with a Kolmogorov power law spectrum. They concluded that the measured sizes result from interstellar scattering which is strongly non-uniform.

Among the OH masers measured in these VLBI experiments, several are unresolved to the limit of angular resolution. Slysh et al. (1996) used a 3-station VLBI network to measure the angular size of three such compact OH masers. With a fringe separation of 4.2 milliarcsec and high signal to noise ratio data the angular size of several spectral features in the two main line OH transitions were measured simultaneously. The measured angular size was in the range from  $1.4 \pm 0.4$  milliarcsec to  $4.3 \pm 0.1$  milliarcsec. It was found that the angular size of the spectral features with the same radial velocity, presumably originating in the same region, was larger in the 1667 MHz line than in the 1665 MHz line. This cannot be the result of scattering, since the scattering size should be virtually the same at these two close frequencies (the scaling between 1665 MHz and 1667 MHz is negligible!). It was concluded that the measured angular size at 1667 MHz  $4.3 \pm 0.1$  milliarcsec for OH34.26+0.15 and  $3.5 \pm 0.2$  milliarcsec for W48 is intrinsic to the sources. These two masers together with OH45.47+0.13 exhibit an angular size for spectral features which is much less than the average broadening estimated from pulsar measurements. The conclusion of that study was that the distribution of the scattering material in the Galaxy is patchy, and that these three masers are located in a direction of low interstellar scattering. For this reason these masers were selected for space-VLBI measurements using the Japanese satellite *HALCA* and a ground telescope array. In this paper we report the first results of the space-VLBI observations of OH maser OH34.26+0.15.

**Table 1.** List of the telescopes used in the experiment.

Station		$T_{sys}$ K	Gain K Jy <sup>-1</sup>	rms Jy
<i>HALCA</i>	(satellite)	88	0.0043	—
Australia Telescope	(Australia)	40	0.667	0.58
Bear Lakes	(Russia)	72	0.54	0.41
Mopra	(Australia)	40	0.1	0.61
Shanghai	(China)	86	0.060	1.35
Tidbinbilla	(Australia)	41	0.9	0.51
Usuda	(Japan)	70	0.797	0.46

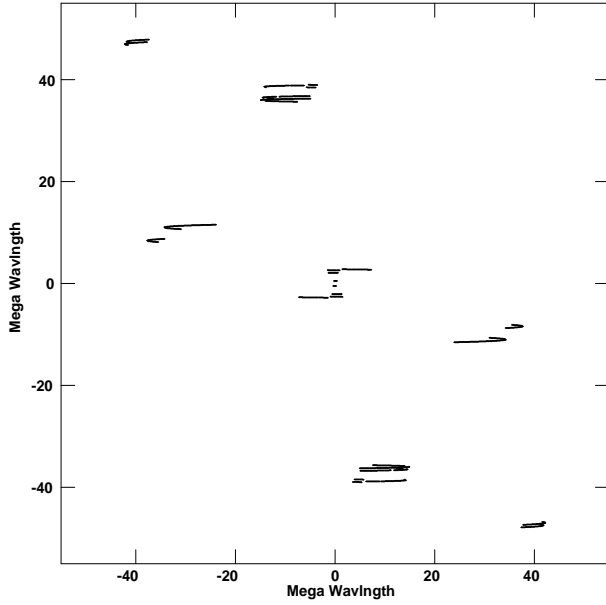
## 2 OBSERVATIONS AND DATA REDUCTION

The maser source OH34.26+0.15 was observed as a part of the Key Science Program of the Japanese Satellite *HALCA* on March 24-25, 1998, by the space-ground very long baseline interferometer. The satellite radio telescope has an 8-m diameter deployable parabolic mirror and uncooled L-band receiver, orbiting the Earth with a 6 hour period, apogee 21000 km and perigee 560 km (Hirabayashi et al. 1998). The ground radio telescope array in this particular session included the 70-m DSN telescope Tidbinbilla in Australia (Tid), the phased 6×22m Australia Telescope (AT), the 22-m Mopra Telescope in Australia (Mop), the Shanghai 25-m Telescope in China (Sh), the 64-m Telescope in Usuda Japan (Usu), and the 64-m Telescope in Bear Lakes (BL) near Moscow (Russia). It was the first time that the Bear Lakes Telescope participated in space-VLBI observations. Table 1 is a list of telescopes with their parameters: system noise temperature  $T_{sys}$ , gain and rms noise in *HALCA* to ground telescope baselines after 5 minutes of integration. The uv-coverage of the ground telescope array is shown on Fig. 1a, and the uv-coverage of the full array including the space radio telescope is shown on Fig. 1b. It is evident that the addition of the space radio telescope not only increases the uv-coverage by a factor of two due to the high orbit of the space radio telescope, but also significantly fills the uv-plane coverage at lower resolution due to the orbital motion of satellite. For the ground array the synthesized beam was  $5.8 \times 2.1$  milliarcsec, and for the space-ground array the beam was  $1.8 \times 1.0$  milliarcsec.

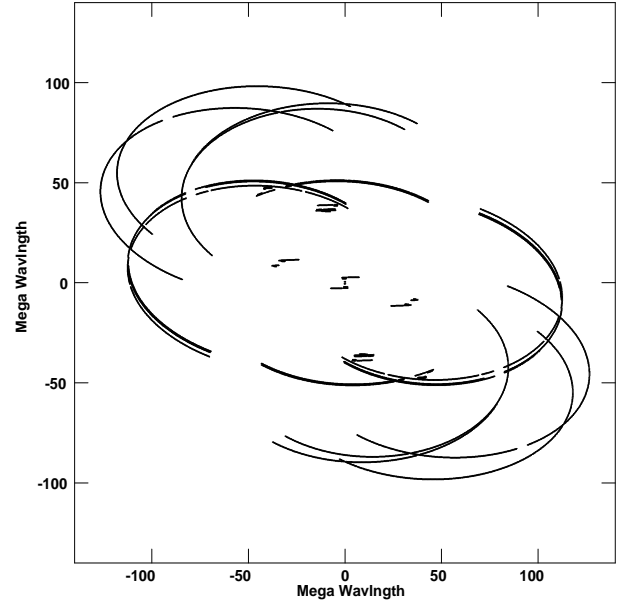
Left circular polarization data over a 16 MHz bandwidth centered on the 1665 MHz and 1667 MHz OH main lines were recorded using S2 recorders at each station. The data were correlated using the Canadian S2 Space-VLBI correlator\* (Carlson et al. 1999). The 16 MHz data were filtered using a FIR bandpass filter and then re-sampled before correlation in order to attain a spectral resolution of 488 Hz channel<sup>-1</sup> ( $0.088 \text{ km s}^{-1}$ ) over a bandpass of 500 kHz. Amplitude calibration was achieved using the “gain” and  $T_{sys}$  data (Table 1) obtained from ground observatories and from the VSOP operations group. The post-correlation data reduction was performed using the AIPS package of NRAO.

Phase jitter was discovered at the Bear Lakes telescope which caused splitting of the fringe spectrum into several components. It was found that the phase of the Bear Lakes

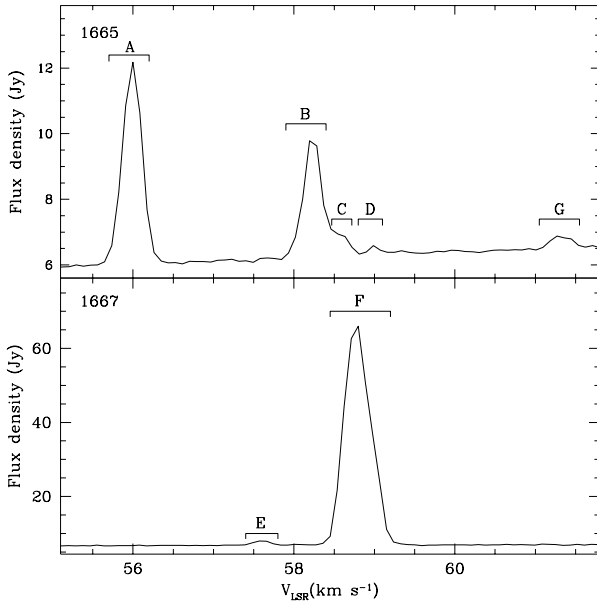
\* The Canadian S2 Space-VLBI correlator at the National Research Centre of Canada, Dominion Radio Astrophysical Observatory is operated by the Canadian Space Agency.



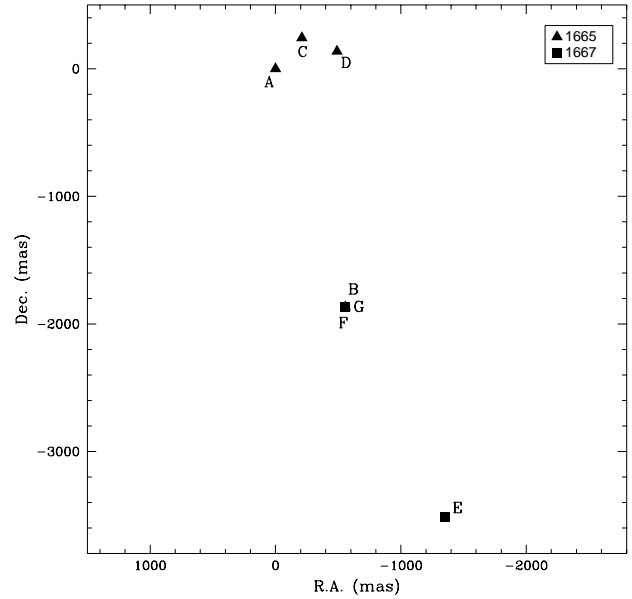
(a) ground array (AT, BL, Mop, Sh, Tid, Usu)



(b) ground array + HALCA

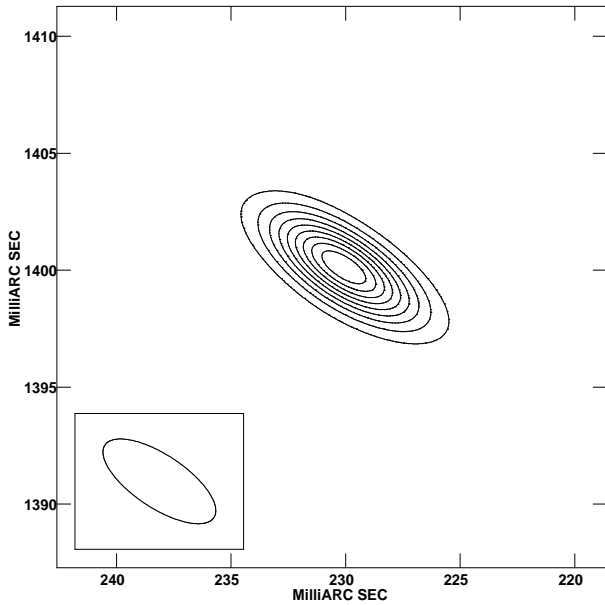
**Figure 1.** uv-plane coverage for OH34.26+0.15. Note different scale for (a) and (b).**Figure 2.** Correlated spectrum of OH34.26+0.15 on the short base line AT–Mopra. Upper panel: the 1665 MHz line; lower panel: the 1667 MHz line.

telescope receiver experienced quasi-periodical excursions with a period of about 200 seconds. The phase jitter was removed by means of phase self-calibration of the ground array with a short solution interval of 30 seconds, which is less than the instrumental, tropospheric and ionospheric phase variation period. The multiple spectral components

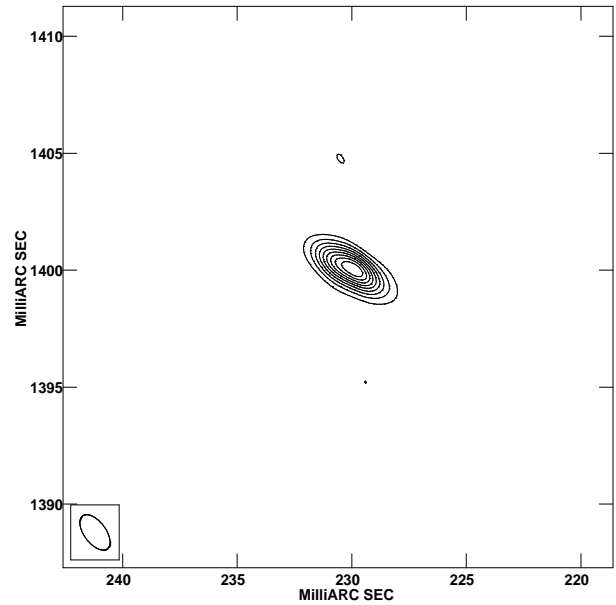
**Figure 3.** Map of OH34.26+0.15. Triangles denote 1665 MHz features, squares are 1667 MHz features. Feature A was taken as a reference (0,0).

disappeared, and the central peak increased by a factor of two.

The strongest and most compact spectral feature at the radial velocity  $56 \text{ km s}^{-1}$  in the 1665 MHz spectrum was taken as a reference in the self-calibration process. Its position relative to the correlating position was determined by the fringe rate method, using the ground array. The mea-



(a) ground array map. Contours are  $0.971 \times (1, 2, 3, 4, 5, 6, 7, 8, 9)$  Jy/beam



(b) ground array + *HALCA*. Contours are  $0.577 \times (1, 2, 3, 4, 5, 6, 7, 8, 9)$  Jy/beam

**Figure 4.** Map of the 1665 MHz feature A at a radial velocity  $56.0 \text{ km s}^{-1}$ . The synthesized beam is shown in the lower left corner. The offsets are relative to the correlating position:  $\alpha = 18^{\text{h}}53^{\text{m}}18^{\text{s}}.67$ ,  $\delta = 01^{\circ}14'58''.5$  (J2000.0)

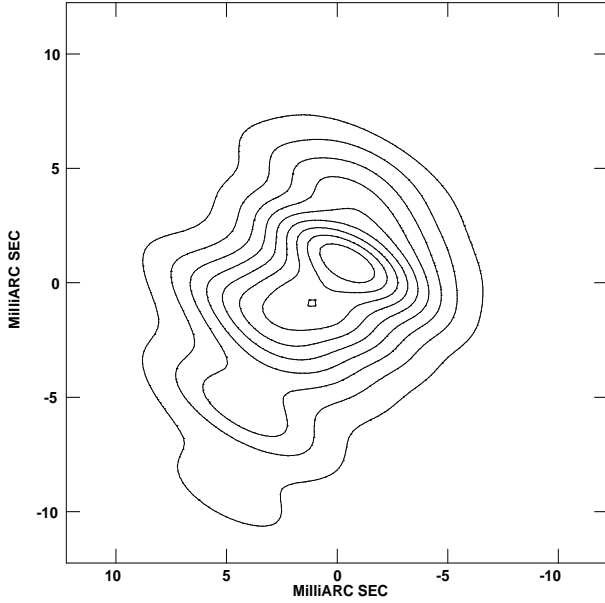
sured offset is  $0''.23$  in right ascension and  $1''.4$  in declination, with an accuracy of  $0''.1$ , and our best position for this feature is  $\alpha = 18^{\text{h}}53^{\text{m}}18^{\text{s}}.685$ ,  $\delta = 01^{\circ}14'59''.9$  (J2000.0). The position of the reference feature A determined here differs from the measured with the VLA by Gaume & Mutel (1987) by about  $0''.15$  in both coordinates, which is within the combined error limits of the two measurements. After applying this correction the residual fringe rate on all base lines including those to *HALCA* was found to be close to zero, and the phase variations became slow enough to allow integration time up to 5 minutes.

The delay errors for the ground array telescopes were measured to be less than 300 nanoseconds from observation of the continuum calibration source 1730–130, which was observed during the time interval when *HALCA* was not observing. The maximum residual delay associated with the baselines to *HALCA* obtained during correlation of the experiment using the Penticton Correlator, which assumed an accurate *HALCA* orbit and other known a priori information, was less than 300 nanoseconds at both 1665 MHz and 1667 MHz. Thus, any additional delay errors after correlation are unlikely to be larger than 300 nanoseconds which will produce a negligible phase difference over the  $5.3 \text{ km s}^{-1}$  spread across maser lines.

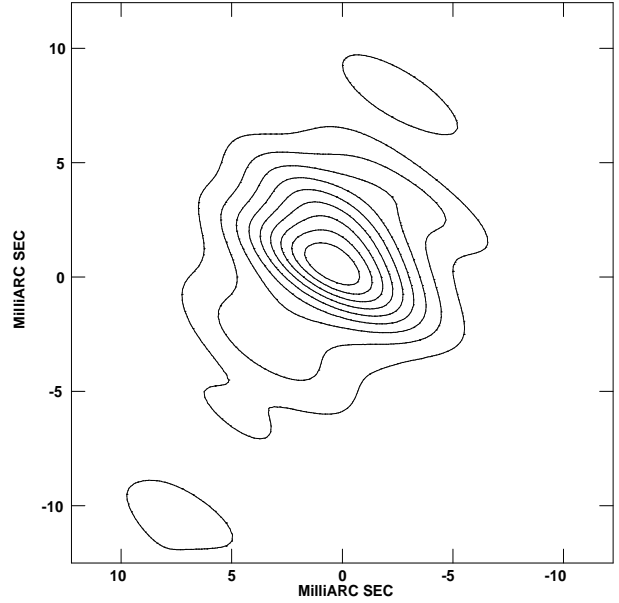
The relative positions of the 1665 MHz line maser spots with respect to feature A were determined in two steps. First, an approximate position relative to the reference feature was measured by the fringe rate method with the ground array. These measurements provided positions with an accuracy of about 50 milliarcseconds, with relative displacements of the features reaching 2000 milliarcseconds. Then maps of the separate features were constructed cen-

tered on these approximate positions, with the ground only or space-ground array when the signal to noise ratio was large enough. The features mapped by the space-ground array are marked by stars in Table 2. The imaging and cleaning were done with the AIPS task “IMAGR”, and the features were analyzed with the AIPS task “SAD” from which the flux density, position and deconvolved size (or size limit) were obtained for each feature. The relative positional accuracy is about 1 milliarcsecond. Result of this analysis is given in Table 2, where for each Gaussian component are given: radial velocity, relative position, flux density, angular size of the major and minor axis of deconvolved Gaussian components as well as position angle of the major axis.

The 1667 MHz OH line data were reduced in the following manner. The  $58.70 \text{ km s}^{-1}$  feature in F is the strongest feature and that was used as the phase reference. Images of the other features in F and feature E (after using fringe-rate mapping to determine its approximate position), were then made by imaging and cleaning as for the 1665 MHz line. In order to tie the 1665 MHz and 1667 MHz images to one coordinate system, we assumed that feature E at 1667 MHz was at the position  $(-1350, -3530)$  milliarcseconds displaced from feature A at 1665 MHz, following Gaume & Mutel (1987). This registration should be accurate to about 50 milliarcseconds. The near coincidence of 1665 MHz features B and G with that of F at 1667 MHz is independent evidence that this registration is accurate.



(a) Map of the 1665 MHz feature B. Contours are  $0.10 \times (1, 2, 3, 4, 5, 6, 7, 8, 9)$  Jy/beam



(b) Map of the 1667 MHz feature F. Contours are  $2 \times (1, 2, 3, 4, 5, 6, 7, 8, 9)$  Jy/beam

**Figure 5.** Maps of the 1665 MHz feature B and 1667 MHz feature F.

**Table 2.** Spectral features

	Velocity	$\Delta\alpha$	$\Delta\delta$	Flux	Size		PA
	$\text{km s}^{-1}$	milliarcsec	milliarcsec	density	maj	min	$^{\circ}$
				Jy	milliarcsec	milliarcsec	
1665 MHz							
A	56.0	0	0	10.5	2.0	<0.5	70
B	58.15	-553	-1873	0.6	3.6	2.7	88
	58.15	-557	-1867	2.9	5.9	2.4	156
	58.19	-553	-1869	0.6	<2.7	<2.7	—
	58.25	-528	-1864	0.6	3.1	1.7	33
C	58.63	-210	242	2.1	3.1	0.2	70
D	58.98	-491	137	1.7	<1.8	<1.8	—
G	61.30	-553	-1866	1.0	1.6	0.6	88
1667 MHz							
E	57.63	-1350	-3530	4.5	5.0	2.9	150
F	58.65	-550	-1890	19.7	6.8	2.8	155
	58.70	-553	-1888	21.3	<2.5	<2.5	—
	58.75	-553	-1885	19.7	5.1	1.8	112
	58.95	-549	-1836	19	6.5	4.1	170

1 – reference position of A is  $\alpha=18^{\text{h}}53^{\text{m}}18^{\text{s}}685$ ;  $\delta=01^{\circ}14'59''.9$  (J2000.0)

2 – Reference position of E for 1667 MHz is  $(-1350, -3530)$  milliarcseconds with respect to A.

### 3 RESULTS

The correlated LCP spectra of OH34.26+0.15 on the short Australia Telescope – Mopra baseline on which the source is unresolved, in both main line OH transitions is shown in Fig. 2. Five spectral features A–D and G are present in the 1665 MHz spectrum, and two features E and F in the 1667 MHz spectrum; their relative position is shown

in Fig. 3. Fig. 4a shows a map of feature A obtained with the ground array. The feature is unresolved with a synthesized beam of  $5.8 \times 2.1$  milliarcsec (lower left corner). Fig. 4b shows a map of the same feature A obtained with the space-ground array having a synthesized beam of  $1.8 \times 1.0$  milliarcsec (lower left corner). The feature is partly resolved, and this is evident from the different position angles of the beam and the image. A deconvolved fitted Gaussian to this image is an ellipse at a position angle of  $70^{\circ}$ , with the major axis 2.0 milliarcsec and the minor axis equal to or less than 0.5 milliarcsec. Inspection of Table 2 shows that all components are partly resolved with the beam of the space-ground or ground only array, but most of the components may have structure and consist of several smaller components.

Other 1665 MHz spectral features are offset from the reference feature by up to  $1''.9$ , their position is shown in Fig. 3. Feature B consists of four separate closely spaced spots as can be seen on the map (Fig. 5a) and in Table 2, where radial velocity, relative position, flux, and angular size of all spectral features are given. Feature F (1667 MHz) coincides with feature B within the measurement errors, and its shape is similar to the shape of feature B (Fig. 5). These two features may come from the same maser condensation, a supposition that can be tested with higher accuracy relative 1665/1667 position measurements. If this is the case the radial velocities of features B and F must coincide, and the observed velocity difference of  $0.5 \text{ km s}^{-1}$  can be attributed to a difference between Zeeman splittings of 1665 MHz and 1667 MHz lines because of different g-factors of two transitions. If the observed features B and F are  $\sigma$ -components of Zeeman pairs (both are left circular polarized), one can calculate that the velocity difference of  $0.5 \text{ km s}^{-1}$  corresponds

to the magnetic field of  $B=4.2$  milligauss, which is a value commonly found in OH masers (Garcia-Barreto et al. 1988).

## 4 DISCUSSION

### 4.1 Maser spot distribution

OH34.26+0.15 is located at a distance of 3.8 kpc (Reid & Ho 1985) near a cometary H II region and near two ultra-compact H II regions. Maser spots A, C and D coincide with the northern ultra-compact H II region G34.3+0.2B, while spots B, E, F and G coincide with the cometary H II region G34.3+0.2C (see Fig. 7 in Gaume, Fey and Claussen 1994). Our map of OH components (Fig. 3) is consistent with the VLA map of the same source obtained by Gaume & Mutel (1987) in 1985. All components A–E have their counterparts on the Gaume & Mutel (1987) map, except component D. On the other hand, some weaker components from the map of Gaume & Mutel (1987) are not present in our map. The splitting of components B and F into four subcomponents is not evident on the Gaume & Mutel (1987) map because of the much lower resolution of the VLA. The relative position of the components on both maps is the same within the VLA position error of about 50 milliarcsec, while the relative positional errors in our map are about 1 milliarcsec. The mean difference in position is  $5.5 \pm 25$  milliarcsec.

### 4.2 Resolution of the feature A

The most compact component is feature A, which is known to be left hand circularly polarized (Caswell & Haynes 1983). It was resolved in one direction, and the angular size in this direction is 2.0 milliarcsec and less than 0.5 milliarcsec in the perpendicular direction. Feature A was fitted with an ellipse in position angle  $70^\circ$  with the ratio of major to minor axis greater than 4. This size is a result of the fitting and deconvolution with the beam of the image shown in Fig. 4b. As an almost independent check of the size of feature A we made a direct fit of a Gaussian model to uv-data using only fringe amplitude information. This procedure is independent in the sense that it does not use the self-calibration and global fringe fitting. The best fit to fringe amplitudes from three telescopes AT, Tid and *HALCA* was achieved with an elliptical Gaussian, having major and minor axis  $2.6 \pm 0.5$  and  $0.3 \pm 0.3$  milliarcsec and a position angle  $61.5 \pm 3.2^\circ$  which, within the errors, is the same as obtained from the image. From our data it is not possible to say whether maser spot A has a stripe-like shape, or is composed of a chain of point-like sources. To determine this, one needs higher angular resolution and higher signal to noise data in order to obtain maps with a higher dynamic range.

In this experiment we could not use the full angular resolution of the space-ground array because of the limitations set by the signal to noise ratio of the data. While the orbit of *HALCA* provided uv-distances up to 135 M $\lambda$ , the fringes were lost in the noise every time the uv-distance from a ground telescope to the space telescope exceeded about 90 M $\lambda$ . This can be seen in Fig. 6, where we show fringe amplitude and phase versus time for the baseline AT–*HALCA*. During the session the uv-distance first increased

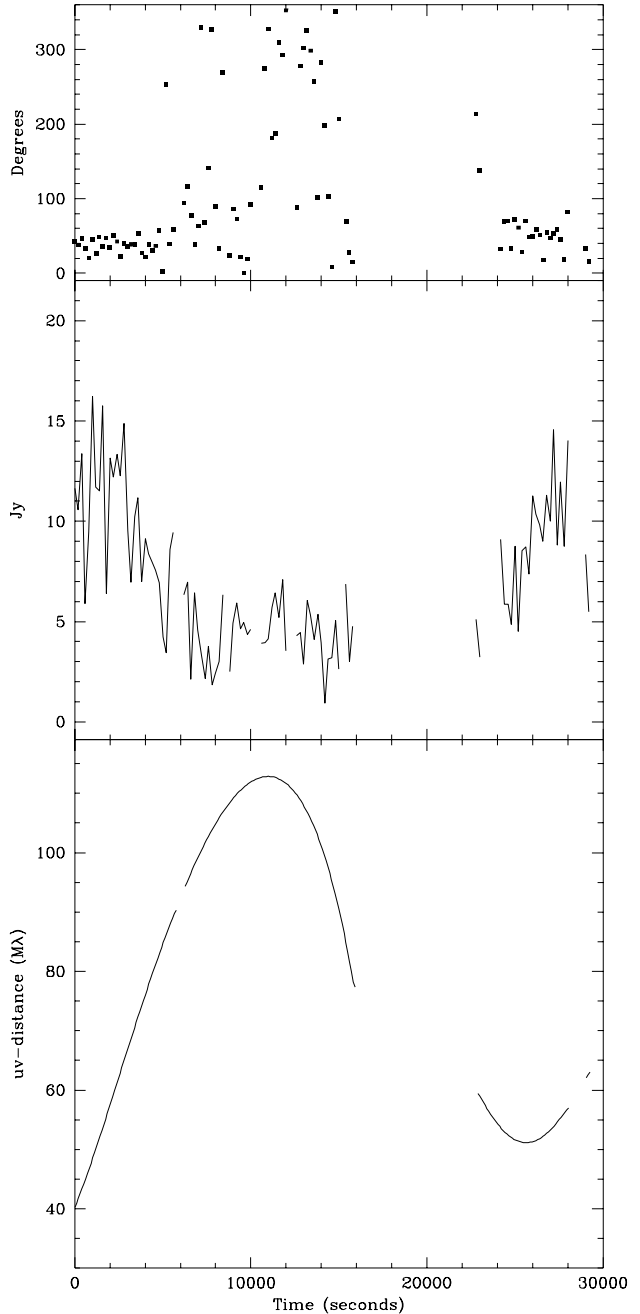


**Figure 6.** Fringe amplitude and phase versus time for feature A on the baseline AT–*HALCA*. Upper panel – phase, middle panel – amplitude, lower panel – uv-distance.

from 40 M $\lambda$  and reached a maximum of 113 M $\lambda$  at 11000 seconds, then decreased to 78 M $\lambda$  at 16000 seconds. It is evident from Fig. 6 that the fringe amplitude has decreased from about 12 Jy to less than 4 Jy which is below the noise level. This can be seen from the phase behaviour in the upper panel of Fig. 6: the phase varies smoothly from 0 to about 6000 seconds (about 90 M $\lambda$ ), and then becomes chaotic. The smooth phase variation resumes during the second portion beginning at about 23000 seconds, up to the end of this session. During the second portion the uv-distance was between 51 and 64 M $\lambda$  and the fringe amplitude was above the noise.

This example shows that the low signal to noise ratio prevents us from using the full angular resolution available. If the signal to noise ratio were increased by a factor of 3 it would be possible to implement full angular resolution imaging. The main cause of the low signal to noise ratio is the small size of the space radio telescope. An increase in the signal to noise ratio by a factor of three would require an increase in the space telescope diameter by the same factor, or a combination of larger diameter and lower system noise temperature.

The upper limit of the angular size of feature A cited above corresponds to the lower limit of its brightness temperature of  $6 \times 10^{12}$  K. Other features have somewhat larger sizes and lower brightness temperature limits, although it cannot be excluded that they consist of several unresolved subcomponents. This value exceeds the brightness temperature predicted by some OH maser models. For example a model by Pavlakis & Kylafis (1996) predicts brightness temperatures about  $10^{11}$  K, or at least an order of magnitude lower than observed. On the other hand there is an absolute upper bound to the brightness temperature imposed by the stimulated transition line broadening (or resonant Stark effect (Slysh 1973)). The stimulated emission rate  $R$  is

$$R = \frac{\Omega}{4\pi} \frac{kT_B}{h\nu} A = 889 \frac{\Omega}{4\pi} \times T_{B12} \text{ s}^{-1} \quad (1)$$

where  $\frac{\Omega}{4\pi}$  is maser emission solid angle,  $A$  is the spontaneous emission rate ( $7.11 \times 10^{-11} \text{ s}^{-1}$  for 1665 MHz OH transition), and  $T_{B12}$  is the brightness temperature in units of  $10^{12}$  K. For feature A the stimulated emission rate  $R = \frac{\Omega}{4\pi} 5.4 \times 10^3 \text{ s}^{-1}$ , and is comparable to the observed line width which is  $0.33 \text{ km s}^{-1}$ , or  $1.6 \times 10^3 \text{ Hz}$ . For an isotropic maser  $\Omega = 4\pi$ , and the contribution of the stimulated emission to the line width is  $\frac{R}{2\pi} = 8.5 \times 10^2 \text{ Hz}$ , or about a half of the linewidth. This means that the brightness temperature can not be much higher than the observed upper limit  $6 \times 10^{12}$  K, unless the maser emission is highly directed. For example, if  $\frac{\Omega}{4\pi} = 10^{-2}$ , the brightness temperature can be as high as  $6 \times 10^{14}$  K. Since the maser lines do not show any measurable broadening the maser is probably anisotropic.

Elongated shapes of OH masers features are also seen in other sources. Baudry & Diamond (1998) found a filamentary and arc-like structure in the OH maser W3(OH) at 13.44 GHz. They relate this structure to a shocked environment of the ultra-compact H II region. One can also speculate that the elongated filaments were formed as a result of an anisotropic compression of the molecular gas into dense condensations in the presence of the magnetic field which is observed in OH masers through Zeeman splitting and polarization of emission lines.

### 4.3 Interstellar scattering

OH masers connected with regions of formation of massive stars are located in the plane of the Galaxy, and are subject to strong interstellar scattering. As a result of scattering, the image of small sources is broadened to an extent that depends on the level of turbulence that produces scattering electron density inhomogeneities. The observed small angular size of maser spots in OH34.26+0.15 puts a strong upper limit on the turbulence level which is usually characterized by a constant  $C_N^2$  in the turbulent electron density power

spectrum. The scatter-broadened angular size is related to the so-called scattering measure

$$SM = \int_0^L C_N^2 ds, \quad (2)$$

where the integral is over distance  $s$  up to the source at distance  $L$ . For galactic sources the scattered angular diameter  $\theta_s$  and  $SM$  are related by the expression (Taylor & Cordes 1993)

$$SM = \left( \frac{\theta_s}{71 \text{ mas}} \right)^{\frac{5}{3}} \nu_{\text{GHz}}^{\frac{11}{3}} \text{ kpc meters}^{-\frac{20}{3}}. \quad (3)$$

If the measured upper limit of the size of the minor axis of component A of 0.5 milliarcsec is due to scattering, and  $\nu = 1.6654 \text{ GHz}$ , then from equation (3) one has

$$SM = 1.68 \times 10^{-3} \text{ kpc meters}^{-\frac{20}{3}}. \quad (4)$$

At a distance of 3.8 kpc this gives  $C_N^2 = 4.4 \times 10^{-4} \text{ meters}^{-\frac{20}{3}}$ . This is almost an order of magnitude less than the average found from pulsar scattering measurements, where  $C_N^2 = 10^{-2.5} \text{ m}^{-\frac{20}{3}}$  (fig. 13 in Cordes, Weisberg & Boriakoff 1985). This means that scattering towards OH34.26+0.15 is much less than the average in the Galaxy.

There exist measurements for interstellar scattering from a nearby extragalactic source 1849+005, which is only  $0^\circ.76$  from OH34.26+0.15 (Fey, Spangler & Cordes 1991). For this source the angular size measured at the frequency 1465 MHz is 560 milliarcsec. Scattering was found to scale with frequency as  $\nu^{-1.65}$  in the range from 333 MHz to 4860 MHz. From pulse broadening, Frail & Clifton (1989) estimated the angular size of a highly scattered pulsar PSR 1849+00 (which is within  $10'$  of 1849+005) as 500 milliarcsec at 1 GHz. If both values are scaled to the OH-line frequency of 1665 MHz, one has 450 milliarcsec from 1849+005 and 216 milliarcsec from the pulsar. These are two to three orders of magnitude larger than the size of the maser spots in OH34.26+0.15. We note that 1849+005 is an extragalactic source, and PSR 1849+00 is a very distant pulsar at a distance of 14.5 kpc (Frail & Clifton 1989). Therefore, the ray path from the sources to the Sun traverses large distances in the Galaxy, with the closest approach to the Galactic Centre of about 4 kpc. The maser OH34.26+0.15 is on the same path, but is much closer to the Sun, at 3.8 kpc. If most of the scattering material lies beyond that distance, presumably near the point where the path is closest to the Galactic Centre (at 6.6 kpc from the Sun, assuming the distance to the Galactic Centre from the Sun 8 kpc), then the OH maser emission will not be scattered so much. One could argue that the large discrepancy of scattering parameters between OH maser and continuum sources (like pulsars) is due to small scale variations in the distribution of the scattering material. The angular separation between the OH maser and 1849+005 is  $0^\circ.76$  and corresponds to 50 pc. This small scale is inconsistent with an almost equally small scattering of two other OH masers in this region OH35.20–1.76 and OH45.47+0.13 (Slysh et al. 1996) which are separated by about  $10^\circ$ , or 650 pc. Based on observations of three low scattered OH masers in the same region, we suggest that there is a large scale deviation in the distribution of the scattering material in the Galaxy.

## 5 SUMMARY AND CONCLUSIONS

We report on the first space-VLBI observations of OH masers. It was also the first time that the 64-m telescope at Bear Lakes near Moscow participated in a space-VLBI experiment. We constructed a map of the maser OH34.26+0.15 with angular resolution better than 1 milliarcsec. The maser consists of small bright spots distributed over several arcseconds, the size of the spots in some cases is less than 0.5 milliarcsec, and the brightness temperature is larger than  $6 \times 10^{12}$  K. This OH maser source experiences an exceptionally small interstellar scattering, and we propose that there is a strong large scale variation in the distribution of the scattering material in the Galaxy.

## 6 ACKNOWLEDGEMENTS

We gratefully acknowledge the VSOP project, which is led by the Japanese Institute of Space and Astronomical Science in cooperation with many organizations and radio telescopes around the world. The National Radio Astronomy Observatory is a facility of the National Science Foundation, operated under a cooperative agreement by Associated Universities, Inc.

## REFERENCES

- Baudry A., Diamond P.J., 1998, *A&A*, 331, 697.  
 Carlson B.R., Dewdney P.E., Burgess T.A., Casorso R.V., Petrichenko W.T., Cannon W.H., 1999, *PASP*, 111, 1025, *astro-ph/9908314*.  
 Caswell J.L., Haynes R.F., 1983, *Aust. J. Phys.*, 36, 417.  
 Cordes J.M., Weisberg J.M., Boriakoff V., 1985, *ApJ*, 288, 221.  
 Fey A.L., Spangler S.R., Cordes J.M., 1991, *ApJ*, 372, 132.  
 Frail D.A., Clifton T.R., 1989, *ApJ*, 336, 854.  
 Garcia-Barreto J.A., Burke B.F., Reid M.J., Moran J.M., Haschick A.D., Schilizzi R.T., 1988, *ApJ*, 326, 954.  
 Gaume R.A., Mutel R.L., 1987, *ApJS*, 65, 193.  
 Gaume R.A., Fey A.L., Claussen M.J., 1994, *ApJ*, 432, 648.  
 Hansen J., Booth R.S., Dennison B., Diamond P.J., 1992, In: Clegg A.W., Nedoluha G.E. (eds.) *Lecture Notes in Physics*, 412, Astrophysical Masers, Springer-Verlag, Berlin, 255.  
 Hirabayashi H. et al., 1998, *Science*, 281, 1825.  
 Kembal A.J., Diamond P.J., Mantovani F., 1988, *MNRAS*, 234, 713.  
 Moran J.M., Burke B.F., Barret A.H., Rogers A.E.E., Carter J.C., Ball J.A., Cudaback D.D., 1968, *ApJ*, 151, L99.  
 Pavlakis K.G., Kylafis N.D., *ApJ*, 467, 309.  
 Reid M.J., Ho P.T.P., 1985, *ApJ*, 288, L17.  
 Slysh V.I., 1973, *Ap. Let.*, 14, 213.  
 Slysh V.I., Migenes V., Kanevsky B.Z., Molotov I.E., Samodurov V.A., Reynolds J.E., Wilson W.E., Jauncey D.L., McCulloch P.M., Feil G., Cannon W., 1996, *MNRAS*, 283, L9.  
 Taylor J.H., Cordes J.M., 1993, *ApJ*, 411, 674.  
 Weaver H., Williams D.R.W., Dieter N.H., Lum W.T., 1965, *Nature*, 208, 29.